ACS Sustainable Chemistry & Engineering

Research Article

Cite This: ACS Sustainable Chem. Eng. XXXX, XXX, XXX−XXX

pubs.acs.org/journal/ascecg

Catalytic Hot-Gas Filtration with a Supported Heteropolyacid Catalyst for Preconditioning Biomass Pyrolysis Vapors

Braden Peterson,*[,†] Chaiwat Engtrakul,*[,‡] A. Nolan Wilson,[†] Stefano Dell'Orco,[§,∥] Kellene A. Orton,[†] Steve Deutch,[†] Matthew M. Yung,[†] Anne K. Starace,[†] Yves Parent,[†] David Chiaramonti,[§,∥] and Kimberly A. Magrini[†]

[†]National Bioenergy Center, National Renewable Energy Laboratory, 15013 Denver West Parkway, Golden, Colorado 80401-3393, United States

[‡]Chemistry and Nanoscience Center, National Renewable Energy Laboratory, 15013 Denver West Parkway, Golden, Colorado 80401-3393, United States

[§]Renewable Energy Consortium for Research and Demonstration − RE-CORD, Viale Kennedy 184, 50038 Scarperia, Florence Italy

[∥]CREAR/DIEF, University of Florence, Department of Industrial Engineering, Viale Morgagni 40/44, Florence 50139, Italy

Supporting Information

ABSTRACT: During ex situ catalytic fast pyrolysis (CFP) of biomass, the separation of reactive char and alkali/alkaline particulates from biomass pyrolysis vapors by hot-gas filtration (HGF) leads to improved vapor stability and quality. HGF in tandem with chemical tailoring (e.g., partial deoxygenation) of the clean pyrolysis vapors, denoted as catalytic hot-gas filtration (CHGF), has the potential to further improve vapor composition by removing reactive oxygen moieties and protect downstream upgrading catalysts from fouling. Downstream upgrading refers to both vapor phase upgrading (e.g., ex situ CFP) and condensed phase upgrading (e.g., hydrotreating). Consequently, CHGF (as a single unit operation) was evaluated for preconditioning pyrolysis vapors for downstream upgrading processes. In order to understand the effective operating conditions that successfully filter and partially deoxygenate pyrolysis vapors, a titania-supported molybdenum heteropolyacid (Mo-HPA/TiO_2) catalyst was studied for use in CHGF. Here, pine pyrolysis vapors were generated in a small pilot-scale pyrolyzer and transferred to a CHGF unit via a continuous-flow slipstream. In the CHGF unit, the pyrolysis vapors were filtered and upgraded over a packed Mo-HPA/TiO_2 catalyst bed. Real-time monitoring and identification of the products formed were achieved by molecular beam mass spectrometry. The results showed that under a hydrogen-rich environment, the pine vapors were partially deoxygenated and alkylated over the Mo-HPA/TiO_2 catalyst. Reactivity studies revealed that an increase in hydrogen concentration and a reduction in weight-hourly space velocity enhanced deoxygenation and alkylation. Time-on-stream (TOS) studies showed stable product formation up to 1 h with little change in catalyst activity. Additionally, the liquid product was collected using a custom fractional condensation unit (built in-house) and analyzed by gas chromatography mass spectrometry to confirm that the product was partially deoxygenated and alkylated. The combination of CHGF and fractional condensation allowed for chemical and physical removal of both foulant and value-added compounds (e.g., phenols, alkylphenols, methoxyphenols, cyclopentenones) for additional enhancement of downstream upgrading processes. The pre- and postreaction catalysts were characterized using temperature-programmed desorption, N_2 physisorption, and elemental analysis with results indicating some catalyst coking. A hydrogen-based catalyst regeneration procedure restored the reacted catalyst activity to that of fresh Mo-HPA/TiO_2.

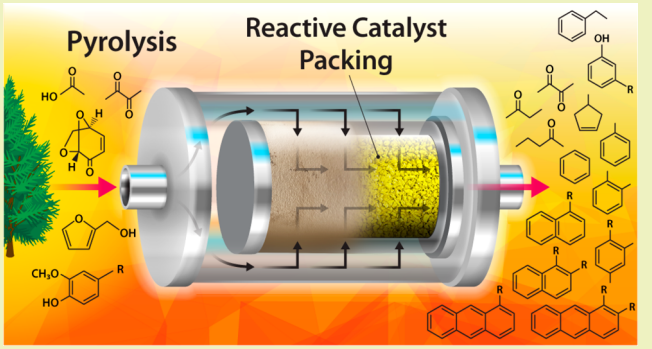

KEYWORDS: *Biomass pyrolysis vapors, Catalytic hot-gas filtration, Hot-gas filtration, Heteropolyacid, Keggin-type structure, Preconditioning, Process intensification, Partial upgrading, Fractional condensation, Separation*

INTRODUCTION

Catalytic fast pyrolysis (CFP) of biomass has the potential to produce valuable end-products and intermediates for the production of renewable liquid fuels and chemicals. This conversion process integrates rapid thermal depolymerization of biomass (fast pyrolysis) with catalytic upgrading to yield desirable products.[1−7] Significant advances in heterogeneous catalysis for bio-oil upgrading via CFP have been made but

Received: June 5, 2019
Revised: August 9, 2019
Published: August 13, 2019

DOI: 10.1021/acssuschemeng.9b03188
ACS Sustainable Chem. Eng. XXXX, XXX, XXX−XXX

there is a continuing need for new catalytic processes and chemistries in order for CFP to be successfully deployed.[8] One of the main challenges associated with CFP is catalyst deactivation due to coke formation, which ultimately leads to biogenic carbon loss.[8−10] The formation of coke is strongly influenced by feed composition. Char and residual alkali metals (particulate matter) are known to catalyze polymerization reactions in both vapors and condensed oils, accelerating coke formation and bio-oil instability, respectively.[8,11−15] Recently, the importance of removing the char and alkali metals from biomass-derived fast pyrolysis vapors was highlighted by demonstrating that hot-gas filtration (HGF) was able to produce a bio-oil with substantially improved properties (i.e., greatly reduced particulate matter including alkali metals).[12,16,17] Additionally, a significant portion of the biomass-derived pyrolysis vapors has reactive oxygen moieties such as acid carbonyls (e.g., acetic acid), which tend to negatively impact CFP due to their corrosive properties. These corrosive acids promote coking reactions (leading to carbon loss) and poor bio-oil stability with respect to storage.[11,14,18−20] Catalytic deoxygenation reactions for the conversion of corrosive acids to more desirable products have been identified in CFP (e.g., decarboxylation). The ketonization of carboxylic acids is a feasible reaction pathway for upgrading biomass-derived pyrolysis vapors and suppressing the formation of corrosive acids while achieving additional carbon−carbon coupling chemistry (i.e., compounds with higher heating values).[19−21] It is important to note that decarboxylation and ketonization reactions tend to remove oxygen from carboxylic acids as CO_2.[20,22,23] This loss of carbon ultimately lowers the carbon efficiency of the conversion of biomass to liquid fuel products. For maximizing fuel yield and quality, hydrodeoxygenation (HDO) is the preferred reaction route since oxygen is eliminated as water and carbon is retained.[8] HDO further presents an opportunity for incorporating hydrogen into end-products prior to hydrotreating, thereby mitigating downstream hydrotreating severity. In order to expand the types of potential catalysts to achieve the desired chemistry, it may be necessary to precondition the vapors with advanced separation processes before downstream catalytic upgrading.

Preconditioning strategies (e.g., partial deoxygenation) have the capacity to chemically convert specific components of biomass-derived pyrolysis vapors to more amenable compounds for CFP. Efforts have been made to integrate catalytic components into hot-gas filter elements used in biomass gasification and gas reforming processes.[24−33] These efforts utilized metal-impregnated (e.g., nickel, ruthenium) ceramic filter elements, with or without mixed-metal oxides (e.g., alumina, zirconia, CaO) incorporated, to both remove particulates and reform tars and light hydrocarbons to synthesis gas (H_2 + CO). Our approach here is to apply hot-gas filtration with an integrated catalytic component to biomass pyrolysis vapors. Denoted as catalytic hot-gas filtration (CHGF), this approach was taken to capture char and alkali metals while simultaneously performing partial deoxygenation and alkylation (i.e., carbon−carbon coupling) on pyrolysis vapors prior to ex situ CFP upgrading. The effect of reaction conditions on the concentration of partially upgraded product vapors was studied. This single unit operation has the potential to extend catalyst lifetime, enable efficient downstream processing, and provide low CapEx oil stabilization, while preserving carbon for downstream CFP upgrading and allowing for the production of carbon−carbon coupled species for tailoring the fuel end-product properties. The use of CHGF within CFP may also present an opportunity for eliminating a cyclone separator used to remove entrained solids in fast pyrolysis vapors.[25]

Fractional condensation of biomass pyrolysis vapors has been previously utilized to alter the composition of the condensed phase by removing water, fouling agents, and value-added chemicals.[34−41] Fractional condensation permits additional tailoring of vapors for downstream upgrading through the removal of reactive and high molecular weight components that contribute to catalyst fouling and oil instability. Moreover, the selective removal of value-added components, such as polymer precursors (e.g., phenols, alkylphenols, methoxyphenols, cyclopentenones), by fractional condensation presents an opportunity for offsetting capital costs within a CFP and/or hydrotreating process.[42,43] In this paper, a custom fractional condensation system was utilized to demonstrate the efficacy of the CHGF unit operation. Here, fractions were collected and analyzed to determine the degree of deoxygenation achieved by CHGF. In addition, the effect of condensation conditions on fractionation is discussed. A new approach is proposed to utilize partial deoxygenation and fractional condensation in tandem to control the composition of biomass-derived product for downstream upgrading processes.

EXPERIMENTAL MATERIALS AND METHODS

Biomass and Catalyst Materials. Loblolly pine biomass feedstock was supplied by Idaho National Laboratory for all experiments. The feedstock was provided in nominal size <2 mm with subsequent knife-milling to <1 mm prior to being used. Carbon, hydrogen, and nitrogen (CHN) and proximate analysis indicated the composition of the pine on a dry basis to be 51.0 wt % carbon, 6.2 wt % hydrogen, 0.1 wt % nitrogen, 42.6 wt % oxygen (by difference), and 0.4 wt % ash. The pine was further characterized as 42 wt % cellulose, 21 wt % hemicellulose, and 30 wt % lignin.

Titania-supported molybdenum and tungsten heteropolyacid catalyst materials (Mo-HPA/TiO_2 and W-HPA/TiO_2, respectively) were prepared using standard techniques. Titania (Alfa Aesar, anatase, #44429) was ground and sieved to a particle size of 1.4−2.0 mm. The catalysts were prepared via incipient wetness impregnation of the TiO_2 support using an aqueous solution containing either phosphomolybdic acid hydrate (Sigma-Aldrich, #221856) or phosphotungstic acid (Sigma-Aldrich, #P4006) to obtain an ∼15 wt % HPA loading. The resulting samples were dried at 120 °C for 18 h. These materials possess the well-characterized Keggin-type structure within the class of heteropolyacids (HPAs) and are also referred to as polyoxometalates when in their conjugate anion form.[44] The HPA structure consists of a metal oxide framework surrounding a central heteroatom, in this case phosphorus. The metal oxide framework is comprised of 12 octahedrally coordinated metal clusters (e.g., molybdenum or tungsten) bonded together through oxygen atoms with oxygen linkages to the central heteroatom. These HPA materials were selected based on their HDO and alkylating activity toward pyrolysis model compounds.[45] Similar activity was promoted with molybdenum oxide supported catalysts,[46−49] and it was determined that the redox properties of molybdenum oxide influenced the reaction selectivity.[50−53] Due to the unique redox properties of molybdenum oxide, a reducible support material (i.e., TiO_2) was leveraged in an attempt to further stabilize and tune the activity of the Mo-HPA via a charge-transfer mechanism between the TiO_2 support and HPA.[54]

Pulsed-Flow Lab Scale Experiments for Catalyst Screening. Initial Mo-HPA/TiO_2 and W-HPA/TiO_2 catalyst screening experiments were accomplished via a pulsed-flow lab scale horizontal quartz reactor system coupled to a molecular beam mass spectrometer (MBMS) for real-time analysis of products. The reactor employed a tubular packed-bed geometry (i.e., axial flow path) with 12.7 mm

DOI: 10.1021/acssuschemeng.9b03188
ACS Sustainable Chem. Eng. XXXX, XXX, XXX−XXX

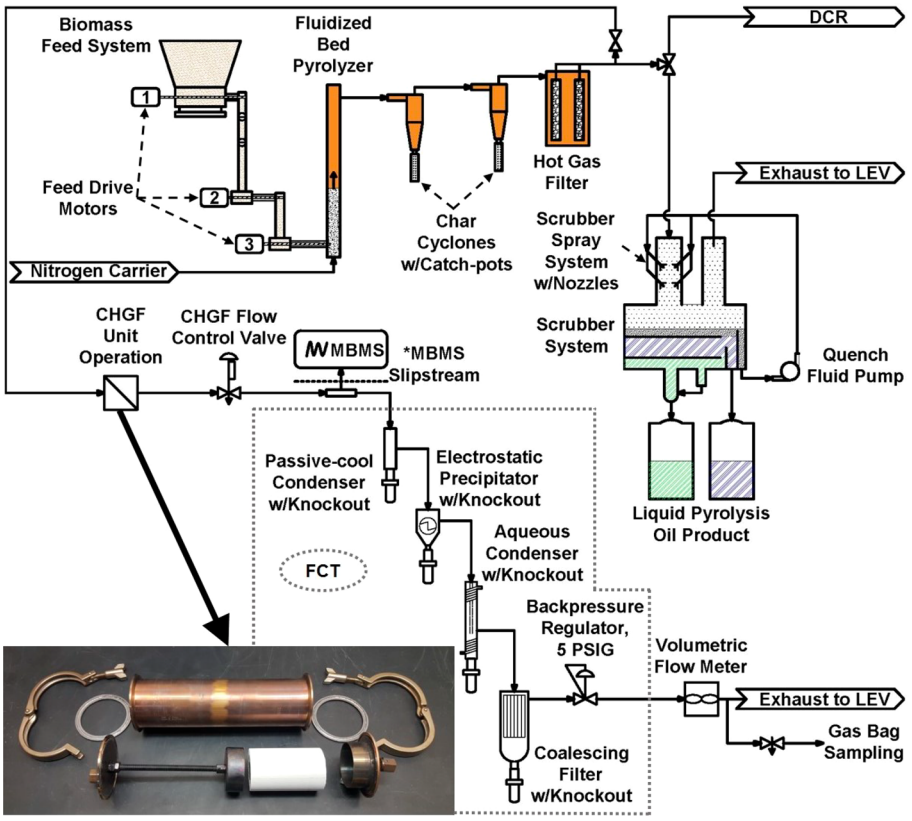

Figure 1. Catalytic hot-gas filter (CHGF) and Davison Circulating Riser (DCR) systems coupled to a small pilot-scale pyrolyzer reactor system. The pyrolyzer system includes a biomass feed system, fluidized bed pyrolyzer, char cyclones + catch-pots, hot-gas filter (HGF) unit, slipstreams to the CHGF and DCR systems, and a scrubber product quench system for raw pyrolysis oil product with liquid phase separation and collection systems. The biomass feed system employs a feed hopper drive (1), a biomass metering drive (2), and a biomass conveying drive (3). The CHGF system is comprised of the CHGF unit operation (shown as inset) housed in a furnace (not shown), CHGF flow control valve, molecular beam mass spectrometer (MBMS) slipstream, and fractional condensation train (FCT). The FCT includes a passive-cool condenser, electrostatic precipitator (ESP), aqueous condenser, and coalescing filter, each with an associated product knockout. The system effluent train is equipped with a backpressure regulator (117 kPa (5 PSIG) setpoint), volumetric flow meter (dry test meter), and gas bag sampling system. Effluent is exhausted to local exhaust ventilation (LEV). *The MBMS system utilized a slipstream via a flow-by plate and was used for real-time analysis of products.

internal diameter and has been detailed elsewhere.[9,55] Pulsed-flow biomass feeding was implemented because of its ease of operation at the lab scale for the catalyst screening experiments. Loblolly pine was pyrolyzed at 500 °C in a flow of He or H_2/He mixture, and the resulting vapors were subsequently upgraded at 400 °C over 0.5 g of catalyst. Resulting upgraded vapors were swept into the MBMS for analysis. Biomass increments of 30 mg were added via quartz boats to give a cumulative biomass-to-catalyst ratio of 1.5 (25 boats) and vapor weight-hourly space velocity (WHSV) of ~2 h^{-1}. Literature regarding the thermocatalytic conversion of lignin model phenolics (e.g., anisole and 4-propylguaiacol) over a Mo-HPA/TiO_2 catalyst suggested that H_2 was necessary to promote HDO and alkylation reactions via Lewis and Brønsted acidic site activation.[45] Therefore, experiments were conducted with 10 vol % and 50 vol % H_2 (balance He). The reaction temperature (400 °C) was chosen based on the thermal stability of the HPA and TiO_2.[56−58] Elevated temperatures (>500 °C) induce a phase transition from anatase-to-rutile, where anatase is the preferred phase. Additionally, pyrolysis vapors tend to condense below 400 °C. All catalyst experiments were tested against corresponding control experiments using only the TiO_2 support. Pulsed-flow lab scale experimental results were used to guide the continuous-flow experiments described in the following section.

Continuous-Flow Experiments Using a Small Pilot-Scale Pyrolyzer and Catalytic Hot-Gas Filtration. As depicted in Figure 1, a custom small pilot-scale fluidized bed pyrolyzer system was employed to pyrolyze biomass at a rate of 1.2 kg/h at 500 °C in a nitrogen (N_2) carrier gas fed at a rate of 1.8 kg/h with ~0.4 kg of additional N_2 purges and operated at 220 kPa (20 PSIG) backpressure (backpressure regulator at the Scrubber outlet not shown in Figure 1). The pyrolyzer consisted of a 5.3 cm internal diameter fluidized bed reactor employing an olivine bed material as a heat transfer media. The system uses a series of two cyclones downstream of the pyrolyzer followed by HGF for char and alkali removal. Subsequently, clean hot-gas filtered pyrolysis vapors could be quenched and condensed in a scrubber or sent to a Davison Circulating Riser (DCR) system as a slipstream for vapor-phase upgrading via CFP.[59] For our study, a pyrolysis vapor slipstream post-HGF was utilized to transfer vapors to a second, smaller, filtration unit operation. This secondary filter setup functioned as a continuous-flow apparatus for CHGF. Experiments employing a pre-HGF slipstream were initially conducted but significant clogging occurred in the transfer line due to char fines entrainment and subsequent deposition. Preliminary results suggested that the pre- and post-HGF slipstream configurations did not significantly affect the pyrolysis vapor composition (data shown in Figure S1 for vapors using TiO_2 control). In addition, complete removal of char and ash using the small pilot-scale HGF was demonstrated and detailed below in the Results and Discussion section. The removal of these components will protect downstream catalyst beds regardless if the catalyst bed is internal to the immediate filter (small pilot-scale HGF) or secondary filter downstream (CHGF). Therefore, utilizing a slipstream post-HGF was suitable for evaluating CHGF. Both the HGF and CHGF unit operations utilized ceramic DiaSchumalith filter elements (filtration grade, 0.3 μm) composed of a silicon carbide inner-core with a mullite (aluminosilicate mineral) outer layer. The cyclones, HGF, and transfer lines were heated to 450, 430, and 400−450 °C,

DOI: 10.1021/acssuschemeng.9b03188
ACS Sustainable Chem. Eng. XXXX, XXX, XXX−XXX

respectively. CHGF was accomplished by the addition of catalyst materials within the core of the filter elements of the slipstream filtration unit operation (Figure 1; see inset). In packing the elements with catalyst material, a decoupling of HGF from partial deoxygenation and chemical conditioning was accomplished, allowing for char and alkali removal prior to partial catalytic upgrading in a single unit operation. Additionally, the CHGF filtration apparatus was coupled to an MBMS for real-time analysis of products followed by a fractional condensation train (FCT) for controlled condensation of liquid products. The FCT (shown in Figure 1 and detailed in Figure S4) was comprised of a passive-cool condenser, temperature-controlled electrostatic precipitator (ESP) with condenser, aqueous condenser, and coalescing filter; all with associated product knockouts. The ESP condenser was operated between 70 and 170 °C with the aqueous condenser at −15 °C and coalescing filter at ambient temperature. Mass flow rate through the CHGF system was controlled using an air-to-close proportioning control valve (CHGF flow control valve). The MBMS and FCT systems were operated at 117 kPa (5 PSIG) with the CHGF operating at 220 kPa (∼20 PSIG), and ∼6.9−13.8 kPa (∼1−2 PSI) differential across the CHGF unit operation with the pyrolyzer marginally above 220 kPa (20 PSIG). The volumetric flow rate of the vapor-stripped effluent from the coupled MBMS-FCT system was measured by a dry test meter. Residual noncondensable gases were captured for off-line analysis via a gas bag sampling system on the MBMS-FCT system effluent.

The continuous-flow CHGF system was comprised of a housing equipped with a mount for securing 102 mm lengths of 60 mm diameter ceramic DiaSchumalith filter elements. Filters were mounted in the housing, and the filter unit was installed in a heated furnace in line with the slipstream transfer line. The flow path was directed from the outside of the filter, inward radially through the filter, and into the packed catalyst bed. All CHGF experiments were conducted at 400 °C with a time-on-stream (TOS) of 60 min using 40 g of Mo-HPA/TiO_2 catalyst. A series of control experiments were conducted prior to upgrading experiments: (1) empty filter housing, (2) filter housing with ceramic filter, and (3) filter housing with ceramic filter packed with TiO_2, all in 40 vol % H_2. The filter elements were then packed with Mo-HPA/TiO_2 catalyst for upgrading experiments. The series of controls followed by catalyst testing allowed for the tracking of incremental changes in the vapor composition throughout the experimental hierarchy of no filter, filter, TiO_2-packed filter, and catalyst-packed filter. Only the Mo-HPA/TiO_2 catalyst material described above was investigated in the continuous-flow catalyst test experiments as the W-HPA/TiO_2 proved to be ineffective based on the pulsed-flow lab scale results (discussed below). Both WHSV and H_2 concentration sweep experiments were conducted with the Mo-HPA/TiO_2 catalyst to investigate the impact of each parameter on activity. Initial testing of the Mo-HPA/TiO_2 at a pyrolysis vapor WHSV of ∼2 h^{-1} with 40 vol % H_2 showed diminished activity compared to the lab scale results obtained at the same WHSV and 50 vol % H_2. Consequently, pyrolysis vapor WHSV was swept from 1−0.25 h^{-1} while the H_2 concentration was swept from 40 to 80 vol %. These parameter sweeps were conducted both independently and simultaneously to determine their individual and combined effects.

Subsequent to the sweep experiments, a triplicate set of Mo-HPA/TiO_2 experiments was conducted to assess reproducibility and mass balance closure. Because the goal was to implement a partial deoxygenation step between pyrolysis and downstream upgrading, the replicate experiments were conducted at the less severe conditions using WHSV of 1 h^{-1}, 40 vol % H_2 at 400 °C, and 60 min TOS. In addition, Mo-HPA/TiO_2 regeneration experiments were conducted using H_2. This protocol (in situ regeneration) entailed flowing 100 vol % H_2 at a flow rate of 300 SCCM over the catalyst at 400 °C for 5 h. The regeneration time was based on the complete removal of the hydrogen-induced desorbed species as monitored via MBMS. Postregeneration, the catalyst was re-evaluated using the same conditions as those used in the replicate experiments above.

Data Acquisition and Analysis. Real-time analysis of products was accomplished via the MBMS slipstream on the CHGF setup. Condensed liquid product from the FCT was quantified gravimetrically and analyzed via GC-MS and Karl Fischer titration while noncondensable gases were analyzed via a GC-FID equipped with a Polyarc universal carbon detector (Activated Research Company). The Polyarc employs a catalytic methanation reaction to convert all GC-separated species into methane prior to FID analysis (i.e., normalizes response factors to 1) to provide for a uniform carbon quantification (i.e., carbon number). The total mass of noncondensable products was determined from the average molecular weight of the product gas, the molar concentration of carbon detected from the Polyarc, and the total volumetric flow through the CHGF system. The average molecular weight of the product gas was determined from the weight fractions and molecular weights of the quantified species. Quenched pyrolysis oil product from the small pilot-scale pyrolyzer was analyzed for alkali metals content via ICP-AES. Mass balances were completed around the replicate experiments by comparing the gravimetric yields of condensable FCT fractions and noncondensable products to those obtained for the filter housing with filter control. The degree of char and alkali removal was assessed gravimetrically through a char and ash balance surrounding the small pilot-scale pyrolyzer and associated HGF system. Both the TiO_2 control and Mo-HPA/TiO_2 materials were analyzed, pre- and postreaction, for metals composition (ICP-AES), surface area (BET), acid site density (NH_3 TPD, combined Brønsted and Lewis acidity), and coke deposition (gravimetrically) to assess reaction-induced changes as they relate to morphology and deactivation. Prior to ICP-AES, BET, and TPD analysis, both pre- and postreaction catalyst materials were calcined in air. The calcination protocol entailed heating in air using a muffle furnace to 550 °C at 3 °C/min, holding for 4 h, and then passively cooling to ambient temperature. Further details regarding the analytical methods employed are provided in the Supporting Information.

RESULTS AND DISCUSSION

Pulsed-Flow Biomass Pyrolysis Vapors: Catalyst Screening Studies. Initial lab scale screening of Mo-HPA/TiO_2 and W-HPA/TiO_2 catalyst materials without hydrogen using a WHSV of pyrolysis vapors of 2 h^{-1} showed limited activity toward pyrolysis vapor deoxygenation or alkylation with rapid deactivation. Both materials produced large amounts of carbon dioxide (m/z = 44) at the expense of primary pyrolysis vapors without any clear changes in oxygenate composition, suggesting thermal and/or catalytic cracking as the primary mechanism for carbon loss. Upon the addition of 50 vol % hydrogen, Mo-HPA/TiO_2 showed a marked increase in activity and stability, while the W-HPA/TiO_2 catalyst showed little improvement. Comparison of catalytic activity between the Mo-HPA/TiO_2 and W-HPA/TiO_2 materials is shown in Figure S2. Due to the inactivity of the W-HPA/TiO_2 material, continued screening experiments focused on Mo-HPA/TiO_2. The Mo-HPA/TiO_2 catalyst exhibited both HDO activity, as evidenced by benzene, toluene, and xylene (BTX) production and alkylation activity based on the appearance of polyalkyl benzenes, naphthalene, anthracene, and their respective alkylated derivatives (methyl and dimethyl). In addition, higher order alkylated hydrocarbons (m/z > 200) were observed (data not shown). Both HDO and alkylation activity appeared to be proportional to the hydrogen concentration. These findings coincide well with those of Anderson et al. for lignin model phenolic compounds.[45] Here, similar HDO and alkylation reactions were promoted when using a polyoxometalate catalyst (conjugate anion of a heteropolyacid) with anisole and 4-propylguaiacol model compounds in a hydrogen environment. Stability experiments for Mo-HPA/TiO_2 (50 vol % H_2) over a cumulative catalyst-to-biomass ratio of 1.5 indicated that little

DOI: 10.1021/acssuschemeng.9b03188
ACS Sustainable Chem. Eng. XXXX, XXX, XXX−XXX

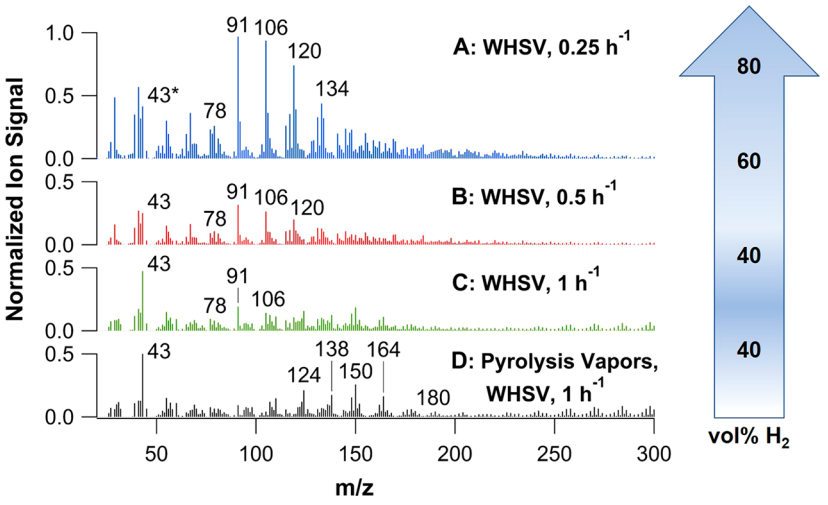

Figure 2. Mass spectra for simultaneous reduction in weight-hourly space velocity (WHSV) and increase in H_2 concentration for (A) partial upgrading of pine pyrolysis vapors with 15 wt % molybdenum heteropolyacid on titania (15 wt % Mo-HPA/TiO_2) using a WHSV of 0.25 h^{-1} and 80 vol % H_2, (B) partial upgrading of pine pyrolysis vapors using 15 wt % Mo-HPA/TiO_2, WHSV of 0.5 h^{-1}, and 60 vol % H_2, (C) partial upgrading of pine pyrolysis vapors using 15 wt % Mo-HPA/TiO_2, WHSV of 1.0 h^{-1}, and 40 vol % H_2, and (D) pure pine pyrolysis vapors (control) at a flow rate equivalent to WHSV of 1.0 h^{-1} and 40 vol % H_2. Carbon dioxide signals (m/z = 44) were similar across spectra and were omitted to reduce the ordinate scale. All experiments were conducted at 400 °C. The m/z values 78, 91, 106, 120, and 134 correspond to benzene, toluene, xylenes, tri-, and tetramethylbenzenes, respectively. The m/z values 124, 138, 150, 164, and 180 correspond to primary vapor products guaiacol, methyl-guaiacol, 4-vinyl-guaiacol, isoeugenol, and coniferyl alcohol, respectively. (*m/z = 43 is a carbohydrate fragment).

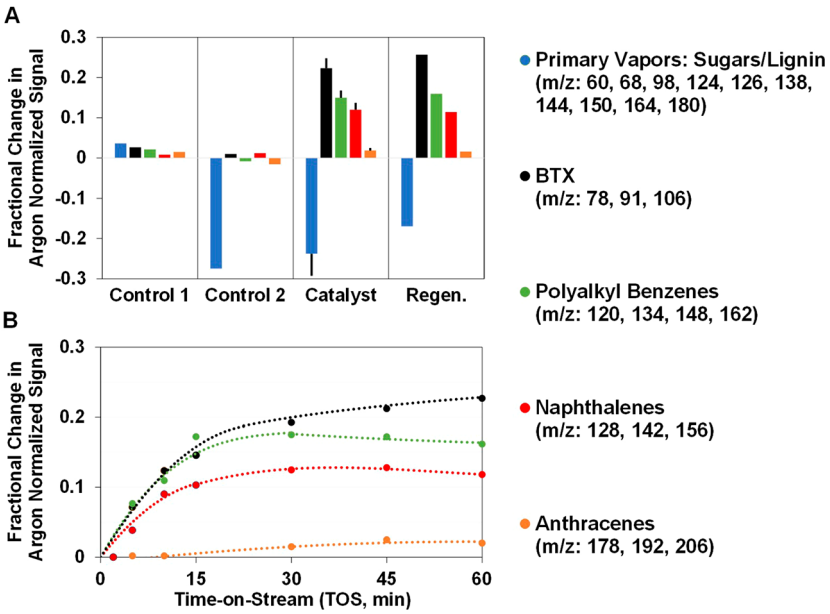

Figure 3. Mass spectra difference data plots for partial upgrading of pine pyrolysis vapors using molybdenum heteropolyacid on titania (15 wt % Mo-HPA/TiO_2) and associated controls. (A) Difference plots showing conversion of primary pyrolysis vapors (sugar- and lignin-derived) to benzene, toluene, and xylene (BTX); polyalkyl benzenes; naphthalenes; and anthracenes upon catalyst addition. Control 1 represents filter housing data subtracted from empty filter data (i.e., Filter − Filter Housing), Control 2 represents empty filter data subtracted from filter + TiO_2 data (i.e., Filter/TiO_2 − Filter), Catalyst represents empty filter data subtracted from filter + Mo-HPA/TiO_2 data (i.e., Mo-HPA/TiO_2 − Filter), and Regen. represents Mo-HPA/TiO_2 − Filter data for H_2-regenerated catalyst. Catalyst experiments were conducted in triplicate with standard deviation bars shown. (B) Time-on-stream (TOS) plot using difference data (Mo-HPA/TiO_2 − Filter) showing trends in BTX, polyalkyl benzenes, naphthalenes, and anthracenes as a function of TOS. Primary pyrolysis vapor difference data was negative and therefore was not shown in TOS plot. All experiments implemented a weight-hourly space velocity (WHSV) of 1.0 h^{-1} and 40 vol % H_2 at 400 °C.

to no deactivation occurred. In fact, the deoxygenated and alkylated products appeared to increase with TOS.

Continuous-Flow Biomass Pyrolysis Vapors: Integration of a Catalytic Component with Hot-Gas Filtration. Continuous-flow pyrolysis vapor experiments using Mo-HPA/TiO_2 with the CHGF system employing the same operating conditions as used in the pulsed-flow studies (i.e., 400 °C, WHSV of ~2 h^{-1}, 40 vol % H_2) showed lower activity. Since hydrogen was constantly flowing during the biomass pulses, catalyst deactivation in pulsed-flow experiments may have been mitigated. Additionally, the difference in flow dynamics between the pulsed- and continuous-flow experiments (i.e.,

DOI: 10.1021/acssuschemeng.9b03188
ACS Sustainable Chem. Eng. XXXX, XXX, XXX−XXX

axial versus radial flow path, respectively) may have contributed to the diminished activity. As shown in Figure 2, a marked improvement in HDO and alkylation activity emerged after decreasing the WHSV to 1 h^{-1}. A progressively higher activity was observed after lowering the WHSV to 0.25 h^{-1}. Activity was also enhanced by increasing the H_2 concentration at a constant WHSV of 1 h^{-1}. Simultaneously decreasing the WHSV of the pyrolysis vapors over the catalyst and increasing the hydrogen concentration resulted in a cumulative effect where activity was further enhanced compared to the independent changes in the two parameters. These results are summarized in a series of MBMS spectra shown in Figure 2: (A) partial upgrading of pine pyrolysis vapors with 15 wt % Mo-HPA/TiO_2, WHSV of 0.25 h^{-1} and 80 vol % H_2, (B) partial upgrading of pine pyrolysis vapors using 15 wt % Mo-HPA/TiO_2, WHSV of 0.5 h^{-1} and 60 vol % H_2, (C) partial upgrading of pine pyrolysis vapors using 15 wt % Mo-HPA/TiO_2, WHSV of 1.0 h^{-1} and 40 vol % H_2, and (D) pure pine pyrolysis vapors (control) at a flow rate equivalent to WHSV of 1.0 h^{-1} and 40 vol % H_2. In decreasing WHSV and increasing H_2, enhanced HDO and alkylation activity were observed with the progressive appearance of benzene (m/z 78), toluene (m/z 91), xylene (m/z 106), and further methylated benzene derivatives (m/z 120 and 134) at the expense of lignin-derived pine pyrolysis compounds (primary vapor products: m/z 124, 138, 150, 164, and 180) produced in the pure pine pyrolysis vapors control (D). Carbon dioxide signals (m/z = 44) were similar across spectra and were omitted to reduce the ordinate scale. These products coincide well with Anderson et al. where methylated benzene derivatives up to pentamethylbenzene and alkylated phenolics were observed for anisole conversion over a titania-supported molybdenum polyoxometalate at 320 °C.[45]

The replicate experiments conducted at less severe conditions (WHSV of 1 h^{-1}, 40 vol % H_2 at 400 °C, and 60 min TOS) demonstrated production of BTX with minor alkylation activity, in accord with the goal of achieving partial deoxygenation prior to additional downstream upgrading. Reasonable agreement in activity between replicate experiments was achieved with results shown as difference plots in Figure 3A. The difference plots were generated from argon-normalized MBMS composite signals. The composite signals were grouped into five categories; sugar- and lignin-derived pine primary pyrolysis vapors, BTX, polyalkyl benzenes, naphthalenes, and anthracenes. Aside from anthracenes, these representative chemical species were selected based on previous literature results.[9,55] The summed sugar- and lignin-derived pine primary pyrolysis vapor species include acetic acid, furan, furfuryl alcohol, guaiacol, 5-hydroxymethyl-furfural or levoglucosenone, methyl-guaiacol, 1,4:3,6-dianhydro-α-D-glucopyranose, 4-vinyl-guaiacol, isoeugenol, and coniferyl alcohol with corresponding m/z values of 60, 68, 98, 124, 126, 138, 144, 150, 164, and 180, respectively. Summed BTX includes benzene, toluene, and xylenes with m/z values of 78, 91, and 106, respectively. The composite naphthalenes and anthracenes signals, including their associated methyl- and dimethyl-derivatives, have corresponding m/z values of 128, 142, 156, 178, 192, and 206, respectively. The degree of HDO activity was assessed on the basis of BTX while alkylation activity can be correlated to the production of toluene, xylenes, polyalkyl benzenes, naphthalenes, and anthracenes.

In Figure 3A, Control 1 represents filter housing MBMS spectral data subtracted from empty filter data (i.e., Filter − Filter Housing), Control 2 represents empty filter data subtracted from filter + TiO_2 data (i.e., Filter/TiO_2 − Filter), Catalyst represents empty filter data subtracted from filter + Mo-HPA/TiO_2 data (i.e., Mo-HPA/TiO_2 − Filter), and Regen. represents Mo-HPA/TiO_2 − Filter data for H_2-regenerated catalyst. Minimal difference is seen between the filter and the filter housing data (Control 1). The minor increase in primary vapors and products may be attributable to thermal cracking in the filter housing experiments since, without a filter present, the housing possesses a greater volume and thus the vapor residence time within the housing is greater. This is substantiated in that oil yield loss was shown via mass balance to be minimal between filter and filter housing experiments (discussed below). A large difference in primary vapors is exhibited between the filter + TiO_2 and the filter data (Control 2) indicating that the TiO_2 support chemically interacts with oxygenates in the pyrolysis vapors. This is thought to be due to the reducible nature of the TiO_2 support. Previously, Zhao et al. demonstrated that oxygen deficient titania (TiO_{2-x}) can be obtained by the thermal treatment of anatase TiO_2 under flowing H_2.[54] The difference between filter + TiO_2 + H_2 and filter + TiO_2 controls (data not shown) indicated minimal changes in vapor composition except for a significant increase in water production (52%). This increase in water suggests that the TiO_2 support was partially reduced under hydrogen. Because of the reducible nature of the TiO_2 support and the redox properties of the Mo-HPA, it is likely that the activity enhancement of the Mo-HPA is occurring due to charge-transfer dynamics between the TiO_2 support and HPA.[19−21,54,58,60−64] The agreement between the triplicate Mo-HPA/TiO_2 experiments in terms of HDO and alkylation activity is evident in that primary pyrolysis vapors were reduced by 23.3 ± 6.2%, BTX increased by 23.2 ± 1.8%, polyalkyl benzenes increased by 15.2 ± 1.9%, naphthalenes increased by 12.6 ± 1.0%, and anthracenes increased by 2.1 ± 0.5%. Intriguingly, acetic acid was reduced by 1.8 ± 0.6%. This was an encouraging result, as acetic acid is known to promote instability in condensed oil products and is a target of the CHGF process for vapor preconditioning prior to downstream upgrading. In addition, H_2-regeneration of the catalyst was effective since results were within statistical variation (Gaussian) of the replicates (Figure 3A).

Figure 3B shows a plot using MBMS difference data (Mo-HPA/TiO_2 − Filter) showing trends in BTX, polyalkyl benzenes, naphthalenes, and anthracenes as a function of TOS. Primary pyrolysis vapor difference data was negative (i.e., reduction in primary pyrolysis vapors) and are not shown on the TOS plot. It is significant to note that this catalyst system was stable under H_2 with no significant indication of deactivation after 1 h of continuous-flow TOS, as evidenced by a continuous increase in the trends for BTX and anthracenes with TOS. Polyalkyl benzenes and naphthalenes also increase to a stable level before decreasing marginally at the end of 60 min TOS. This suggests that hydrogen may not only promote HDO and alkylation activity but balance coke and product formation, thereby stabilizing activity by hindering coke-induced deactivation. As discussed below, it is proposed that hydrogen activation and subsequent reaction with surface-adsorbed intermediates hinders conversion of those intermediates to coke and promotes product formation. Similarly, concomitant generation of water (steam) and subsequent reaction with surface-adsorbed species may further reduce coking.[65] This is further substantiated in Figure S3. Figure

DOI: 10.1021/acssuschemeng.9b03188
ACS Sustainable Chem. Eng. XXXX, XXX, XXX−XXX

Table 1. Characterization of Pulsed-Flow (PF) and Continuous-Flow (CF) Unreacted and Reacted TiO_2 Control and Mo-HPA/TiO_2 Materials with and without H_2

Catalyst ID		ICP-AES, Mo (wt %)	ICP-AES, P (wt %)	Mo-HPA Loading (wt %)	BET Surface Area (m^2/g)	NH_3 TPD (μmol/g)	Catalyst Coke (wt %)
Mo-HPA/TiO_2 (PF)	Reacted w/out H_2						13.4
	Reacted w/H_2						8.5
TiO_2w/H_2 (Control) (CF)	Unreacted				55	365	
	Reacted				67	412	7.2
Mo-HPA/TiO_2w/H_2 (CF)	Unreacted	9.1	0.4	14.4	97	480	
	Reacted	9.2	0.4	14.6	101	497	3.5
Mo-HPA/TiO_2w/H_2 Regen. (CF)	Unreacted	9.2	0.4	14.6	94	432	
	Reacted	9.2	0.4	14.6	96	481	3.2

S3A,B presents MBMS spectra for desorbed products evolved from the postreaction Mo-HPA/TiO_2 catalyst before H_2-regeneration and during H_2-regeneration, respectively, using the same temperature and flow rate conditions. Minimal product evolution was seen under nitrogen while significant amounts of BTX, naphthalenes, anthracenes, and their alkylated derivatives were produced under hydrogen. Because these are the same compounds produced during the CHGF reaction, it is suggested that this coke mitigating mechanism is inter-related with HDO and alkylated product formation and that the two processes utilize similar chemistries. Interestingly, the catalyst material exhibits an induction period for the first ~15 min TOS where the products increase at a rapid rate before leveling off to a steadier rate of increase. This phenomenon needs to be further investigated and may be due to the formation of reactive intermediates on the surface of the catalyst that accumulate prior to developing a steady-state reactive phase. In future studies, catalyst lifetime analysis will be conducted with concomitant regeneration optimization to assess catalyst behavior beyond 1 h TOS for long-term stability. In addition, the potential effect of organic aerosols on the performance of HGF and CHGF was not addressed in this study. It is understood that biomass fast pyrolysis produces aerosols that contain a significant amount of inorganic content (especially potassium and calcium).[66] Under these conditions, it is possible that some of the coking is due to aerosols that pass through the filter media.

Pre- and Postreaction Catalyst Characterization. The proposed hydrogen-based mitigation of coke-induced deactivation is further supported by the reduction in coke on the reacted catalyst in the presence of H_2 as shown in Table 1 for the Mo-HPA/TiO_2 catalyst used in pulsed-flow screening experiments. The coke was reduced from 13.4 to 8.5 wt % with the addition of H_2. Moreover, in hydrogen, a potentiating effect is exhibited for the Mo-HPA/TiO_2 as coke was further reduced on the catalyst relative to the titania support for the materials used in the continuous-flow experiments. Here, coke was reduced from 7.2 to 3.5 wt % with the addition of the Mo-HPA on the titania in H_2. In both instances, it is believed that hydrogen activation on either the TiO_2 and/or Mo-HPA/TiO_2 occurs followed by reaction with surface-adsorbed intermediate species; the resulting hydrogenated products more readily desorb from the catalyst surface, thereby preventing further surface reactions that form coke. Coproduction of steam may further contribute to coke reduction in a similar fashion.[65] This indicates that Mo-HPA promotes H_2 activation in addition to TiO_2, with a synergy potentially experienced between the two materials. Again, this may be due to charge-transfer and redox dynamics between the support and Mo atoms of the Mo-HPA catalyst.[46,52,53] A summary of additional pre- and postreaction catalyst characterization results for molybdenum and phosphorus content, surface area, and acid site density are shown in Table 1. The Mo-HPA loading on the titania support was determined based on the molybdenum content of the samples and the known weight fraction of molybdenum of the Mo-HPA (i.e., $H_3PMo_{12}O_{40}$). The molybdenum and phosphorus content, and therefore the Mo-HPA content, of the catalysts remained unchanged upon reaction. The BET surface area increased upon deposition of the Mo-HPA material on the titania support while it remained unchanged upon reaction for both titania and Mo-HPA/TiO_2 materials. The increased surface area upon addition of Mo-HPA is expected due to the surface area enhancement imparted by the dispersed nanostructured Mo-HPA deposits on the low porosity titania support. The acid site density (combination of Brønsted and Lewis acid sites) of the Mo-HPA impregnated titania support was approximately 100 μmol/g greater than the native titania support. Upon reaction, the acid site density marginally increased for both the support and the Mo-HPA/TiO_2. The reducible nature of and subsequent oxygen deficient site formation on titania is believed to be responsible for this increase in acidity.[54] The stability of these catalyst properties was expected since minimal deactivation was observed during the TOS experiments. These data are in agreement with lignin-derived model compound studies where a reacted molybdenum-based HPA catalyst maintained its Keggin-type structure and did not deactivate appreciably.[45]

A char and ash balance surrounding the small pilot-scale pyrolyzer and associated HGF system was measured gravimetrically. On the basis of these measurements, 98.3 wt % of the char and ash was removed by the two-stage cyclone system with the balance of 1.7 wt % captured by the HGF unit. Within the cyclone system, 97.3 wt % of the char and ash was captured in the first cyclone. Char and ash breakthrough past the HGF unit was not detected while ICP-AES analysis of condensed pyrolysis oil from the small pilot-scale pyrolyzer showed minor quantities of Na, K, Mg, and Ca with values of 6, 20, 54, and 74 ppm, respectively.[12,67−70] Since char and alkali metals have been shown to promote aging of condensed oils through accelerated polymerization reactions,[8,11−15] the ability to remove these materials via cyclonic action coupled with hot-gas filtration is significant. Because the majority of the char and ash was captured in the first cyclone, it is proposed that the second cyclone can be eliminated (Figure 1). According to

DOI: 10.1021/acssuschemeng.9b03188
ACS Sustainable Chem. Eng. XXXX, XXX, XXX−XXX

Dutta et al., the impact of HGF may lead to a capital savings if one of the two cyclones after the fast pyrolysis reactor is eliminated.[25]

Fractional Condensation of CHGF Vapor Products and System Mass Balance. Fractional condensation is a strategy for separating liquid product from vapor phase product conversion streams in a controlled, sequential process. The strategy can be used to separate selected compounds from the organic oil product (ketones, acids, aldehydes), remove heavy oligomeric material, concentrate organic matter, separate the aqueous phase, and isolate coproducts by process control.[71] Oil stability, and therefore oil quality, depends on the ability of reactive oxygen moieties (e.g., acid carbonyls) within the oil to promote aging reactions during storage. The complex mechanisms and pathways associated with oil aging reactions have been described in other studies.[11,18,72−75] Since carbonyl compounds (e.g., aldehydes and ketones) and organic acids (e.g., acetic acid) are the main contributors to oil instability of fast pyrolysis oil,[11,74] an FCT (staged condensation process) was coupled with the CHGF unit operation to reduce the content and distribution of these aging compounds within the organic liquid product. A schematic diagram of the FCT unit is shown in Figure S4.

The hot-gas filtered pyrolysis vapors were condensed in the FCT (shown schematically in Figure 1 and Figure S4) with both qualitative and quantitative analysis conducted on the liquid product samples. The impact of Mo-HPA/TiO_2 catalytic activity on pyrolysis vapor composition is shown in the GC-MS analysis of the condensed oil product as indicated in Figure 4. Figure 4 represents the quantity of GC-detectable

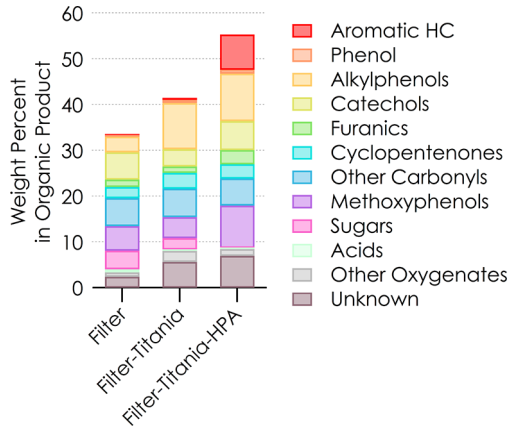

Figure 4. Composition of condensed organic oil product, as determined by GC-MS, for pine pyrolysis vapors partially upgraded via catalytic hot-gas filtration (CHGF) using a molybdenum heteropolyacid on titania (15 wt % Mo-HPA/TiO_2) catalyst. From left to right: empty filter (control) with WHSV 1.0 h^{-1} and 40 vol % H_2, filter + TiO_2 with WHSV 1.0 h^{-1} and 40 vol % H_2, filter +15 wt % Mo-HPA/TiO_2 with WHSV 1.0 h^{-1} and 40 vol % H_2. All experiments were conducted at 400 °C.

compounds per condition, where the increase in GC-detectable compounds when using a catalyst is consistent with upgrading and the concurrent reduction in primary vapors. The change in GC-detectable compounds as a function of upgrading accounts for the lower detectable yield shown in Figure 4 for the filter alone (noncatalytic) since the heavy, nonupgraded species were not detected by the GC method. It is important to note that the group of compounds labeled "Unknown" refers to those compounds that were detected but not identified by the GC method employed. A summary of the oil compositions of CHGF vapors for filter, filter + TiO_2, and filter + Mo-HPA/TiO_2 is provided inTable S1. When the filter was packed with the TiO_2, an increase in the percentage of alkylphenols from 3 to 10 wt % relative to the filter was observed, and this effect was maintained upon the addition of the Mo-HPA (Figure 4). Minor increases in phenol and cyclopentenones were observed using TiO_2. The production of phenol and alkylphenols from biomass using TiO_2 has been reported in the literature.[60,61] While alkylated phenols production was catalyzed by the TiO_2 support, aromatic hydrocarbons and methoxyphenols were further enhanced through the addition of the Mo-HPA to the support (Figure 4). The aromatic hydrocarbon class depicted in the plot comprises 1-ring, 2-ring, and 3-ring aromatic hydrocarbons and alkyl benzenes. These results confirm the real-time MBMS data, which also showed an enhancement of aromatic hydrocarbons and alkylation of aromatic rings along with the production of phenolic compounds. The presence of these upgraded products validates the results obtained in the pulsed-flow lab scale experiments and the scaled-up, continuous-flow system. In addition to hydrocarbons, alkylated phenols and methoxyphenols are chemical classes of interest as value-added chemicals since they are or can be converted to polymer precursors (e.g., phenol, cresols, and xylenols) via further upgrading processes like catalytic hydrodeoxygenation.[42,43] In addition, cyclopentenones and other carbonyls (e.g., aromatic aldehydes or ketones) marginally decreased in the condensed oil and increased in the gas phase (gas bag analysis) with the catalyst addition. The Mo-HPA/TiO_2 in the presence of hydrogen promotes the conversion of acids as demonstrated by the compositional analysis. GC-MS results show a reduction of ∼4 wt % in the collected aqueous phase relative to a blank filter and a ∼ 2 wt % reduction relative to the catalyst support. These results are presented in Table S2.

To further investigate staged condensation of pyrolysis vapors partially upgraded using Mo-HPA/TiO_2, the distribution in mass fractions for several main compound classes (methoxyphenols, ketones and acids) was tracked across different condensation conditions. The product distribution between the fractions depends on vapor pressure, composition, and temperature of the pyrolysis mixture. Moreover, thermodynamic interactions between oxygenated compounds, heat-transfer characteristics of the condenser (tube-in-shell in this case), and residence time of vapor mixture in the heat exchanger can have strong effects on the selective condensation efficiency as mentioned in other works.[71]

Throughout the CHGF-FCT experiments, no product was captured in the first passive-cooled condenser shown in Figures 1 and S4. The class-selective staged condensation was achieved by varying the ESP condensation stage temperature (heat exchanger + ESP) from low (70 °C) to high (170 °C) while keeping the third condensation stage (cold trap) temperature constant at −15 °C. The tube-in-shell heat exchanger used in the third stage cold trap was designed to condense the compounds in the oil according to their dew point, while the ESP stage actively removes entrained aerosols electrostatically and thermally. At 70 °C, the majority of the organic phase was condensed in the ESP second stage while the majority of the aqueous phase was condensed in the third stage cold trap. At the condensation temperature of 170 °C, only sugars (e.g., levoglucosan) were collected in the ESP stage and the oil phase

DOI: 10.1021/acssuschemeng.9b03188
ACS Sustainable Chem. Eng. XXXX, XXX, XXX−XXX

was condensed together with the aqueous fraction contained in the cold trap. In the latter case, the aqueous phase was decanted from this composite oil-aqueous product and the resulting separated oil and aqueous phases were quantified gravimetrically and characterized independently. Fugitive vapors that were not captured in the third stage cold trap were subsequently captured in the coalescing filter as an organic phase. The oil captured in the coalescing filter accounted for <5 wt % of the total product recovered.

The organic phase collected in the second ESP condenser at 70 °C was nearly free of water (1.6 wt % water) as determined by Karl Fischer titration. Coupling CHGF with fractional condensation improved the ability to collect light organic components (<300 °C boiling point). A 42% decrease in heavies (pyrolytic lignin) collected in the heat exchanger (FCT-V-04, in Figure S4) and a 67% increase in light organics (FCT-V-03, in Figure S4) with the ESP condensation stage operated at 70 °C were observed. Separation of the heavy components of pyrolysis vapors is a significant challenge, and the reduction in the heavy component demonstrates the benefit of combining the two unit operations to access chemicals and fuels from pyrolysis vapors. Normalized mass distributions between the ESP condenser and the cold trap of selected classes are provided in Table 2. These results show the ability to shift compounds between liquid products based on temperature. At 70 °C, in the ESP condensation stage (second), the methoxyphenols were condensed primarily in the oil fraction while upon increasing the temperature to 170 °C they were allowed to remain as vapor through the second stage until being condensed in the cold trap. Here, the aqueous and organic phases condensed together as a phase-separated composite. Methoxyphenols have a higher dew point where vapor saturation is reached at higher temperatures (>250 °C), and therefore at 70 °C, the condenser is able to remove them effectively.

Table 2. Mass Distribution of Chemical Classes between the Condenser and the Cold Trap of the Fractional Condensation Train

Chemical Class	Condenser Temperature (°C)	Condenser Product (wt %)	Cold Trap Product (wt %)
Methoxyphenols	70	94	6
	170	0	100
Ketones	70	33	67
	170	0	100
Cyclopentenones	70	59	41
	170	0	100
Carboxylic Acids	70	5	95
	170	0	100
Water	70	<1	>99
	170	<1	>99

As shown in Table 2, slightly different behavior was observed for the ketones when condensed at 70 °C. The total mass of cyclopentenones generated during pyrolysis tended to be distributed evenly between the ESP condenser stage and cold trap. The cyclopentenone compound class has a broad range of boiling points (and therefore dew points) which contribute to the distribution between the two stages. Hence, saturation in the ESP condensing stage could not be achieved for all compounds within the cyclopentenone class. For example, 2-cyclopenten-1-one, 2-hydroxy-3-methyl- has a normal boiling temperature of 253 °C and is completely condensed into the first fraction at 70 °C, while 2-cyclopenten-1-one has a lower normal boiling point (135 °C) and tended to condense within the cold trap. The same reasoning can be applied to the remaining ketones detected with compositional variations in distribution arising from differing dew points among the various ketones. When the condensation temperature was controlled to 170 °C, all the cyclopentenones and the other ketones present in the vapors were completely condensed in the cold trap. The organic acids, including acetic acid, represented ∼5 wt % of the mass collected in the ESP condensation stage at 70 °C. Because these compounds possess low dew points, they remained as vapor at 70 °C and were therefore collected in the cold trap within the aqueous phase. This resulted in a deacidified oil phase in the ESP condensation stage. These results show the difficulty in removing any specific class of compounds in high purity using a simple separation and are in accordance with Rover et al.[76] However, the ability to remove crude fractions of unwanted compounds (e.g., acids) from the organic product through the combined use of partial upgrading via CHGF coupled to fractional condensation was demonstrated and has the potential to enhance oil stability and mitigate downstream CFP and/or hydrotreating catalyst deactivation.

The product distributions obtained for the FCT experiments conducted with CHGF using Mo-HPA/TiO_2 suggest that an average temperature between the two evaluated temperatures (70−170 °C) may be sufficient to isolate the majority of the ketones from the oil, aside from trace-amounts of cyclopentenones. The results further indicate that, for temperatures below 170 °C, the majority of the methoxyphenols can be retained in the organic oil phase within the ESP stage while simultaneously isolating the majority of the acids in the aqueous phase within the cold trap. Controlling product condensation in this fashion allows for the ability to densify, deacidify, and dewater the organic oil phase while concentrating alkylphenols within the same phase. Alternatively, at the higher ESP stage temperature of 170 °C where all upgraded product condensed in the downstream cold trap, the acids and carbonyls partitioned between the oil and aqueous phases; partitioning of reactive carbonyls into the aqueous phase constitutes another means for enhancing oil stability and catalyst lifetime in downstream processes since these species promote aging reactions in the condensed oil phase and catalyst coking reactions in the vapor phase.[75,77] In addition, the heavier aromatic hydrocarbons, alkylphenols, methoxyphenols, and polyalkylated benzenes generated during the upgrading using Mo-HPA/TiO_2 were collected completely in the condensed oil phase within the ESP stage at 70 °C. This demonstrates our intended separation control toward targeted alkylphenols and methoxyphenols as value-added chemicals. Additional stages within the FCT may prove useful in enhancing separations control over targeted cyclopentenones.

The efficiency of the FCT in capturing product was assessed via mass balance using Mo-HPA/TiO_2 CHGF replicates (WHSV of 1 h^{-1}, 40 vol % H_2) with the FCT ESP stage at 170 °C. These data are shown in Table S3 in conjunction with mass balance data for when the FCT ESP stage was at 70 °C. The mass balance closure for the Mo-HPA/TiO_2 replicate experiments was 97.3 ± 3.3 wt % with 45.2 wt % residing as gaseous product, 3.5 wt % lost to catalyst coke, 33.5 wt % aqueous product, and 15.1 wt % as organic oil product. In comparison, the filter + TiO_2 control exhibited a mass balance

DOI: 10.1021/acssuschemeng.9b03188
ACS Sustainable Chem. Eng. XXXX, XXX, XXX−XXX

closure of 96.6 wt % with 48.0 wt % residing as gaseous product, 7.2 wt % lost to catalyst coke, 15.9 wt % aqueous product, and 25.5 wt % organic oil product. The filter control without packing yielded a mass closure of 92.0 wt % with 43.1 wt % gaseous product, nondetectable coke loss, 24.4 wt % aqueous phase, and 24.1 wt % organic oil product. The gas yields were high due to thermal cracking of pyrolysis vapors in the small pilot-scale pyrolyzer system prior to their delivery to the CHGF unit. The pyrolyzer was not optimized for pyrolysis vapor quality prior to experiments. It is anticipated that an optimized pyrolyzer would improve vapor quality by reducing the light gas yield while concomitantly increasing the viable upgradable vapor yield. A reduction in the oil product yield in the Mo-HPA/TiO_2 can be attributed to much of the upgraded product being volatile and not efficiently condensed in the FCT. Partial deoxygenation also removes oxygen as water, evidenced by the increase in aqueous phase when using catalyst. Previous work indicated a negative correlation to oil yield and degree of deoxygenation.[78] It should be noted that the mass balances were comparable for the two ESP stage temperatures investigated (70 and 170 °C).

CONCLUSION

Catalytic hot-gas filtration (CHGF) was successfully used to condition biomass fast pyrolysis vapors provided by a continuous-flow small pilot-scale pyrolyzer unit by integrating a catalytic component based on a heteropolyacid into a hot-gas-filtration (HGF) unit. This CHGF process in combination with a cyclone system produced clean (i.e., no particulates and low alkali metals) and partially upgraded fast pyrolysis vapors for either fractional condensation or downstream catalytic upgrading. Produced vapors contained increased quantities of aromatic and alkylated hydrocarbons. Both hydrodeoxygenation and alkylation reactions were essential in the partial conversion of the pine-derived oxygenates. In the combined process, the removal of alkali metals stabilizes associated pyrolysis and upgraded oils, while the partial deoxygenation (i.e., removal of reactive oxygen moieties) enhances CFP by reducing coke formation and promoting improved oil stability. The efficient capturing of char and alkali particulate at the HGF indicates that a single cyclone for entrained solids removal will suffice, thereby allowing for the elimination of the second cyclone typically employed in ex situ CFP.

The coupling of the catalytic preconditioning of pyrolysis vapors via CHGF with the controlled condensation demonstrated an additional means to enhance oil stability while preserving carbon for downstream upgrading and production of carbon−carbon coupled species for tailoring fuel end-product properties. Controlled condensation provided phase separation between organic oil and aqueous products. Controlled condensation additionally allowed for the targeted condensation of heavy aromatic hydrocarbons, alkylphenols, and methoxyphenols within the oil phase and reactive acid carbonyls within the aqueous phase. On the contrary, the distribution of ketones spanned both the oil and aqueous phases, suggesting that additional FCT stages would be necessary for improving their separation. This chemical tailoring of either vapor phase or condensed phase product composition is a viable option for enhancing downstream upgrading within CFP and/or hydrotreating via foulant removal. Value-added product separation using FCT represents an additional enhancement to the upgrading process; polymer precursors have the potential to offset process capital costs. The CHGF and FCT unit operations together offer a low CapEx approach for enhancing oil stability, product composition, and overall efficiency within CFP processing of biomass fast pyrolysis vapors to selected fuels and chemicals.

ASSOCIATED CONTENT

Supporting Information

The Supporting Information is available free of charge on the ACS Publications website at DOI: 10.1021/acssuschemeng.9b03188.

Experimental method details, catalytic hot-gas filtration, fractional condensation train results including mass balance results for CHGF experiments (PDF)

AUTHOR INFORMATION

Corresponding Authors

*E-mail: braden.peterson@nrel.gov.

*E-mail: chaiwat.engtrakul@nrel.gov.

ORCID

Chaiwat Engtrakul: 0000-0002-8773-0668

A. Nolan Wilson: 0000-0002-9002-3585

Kimberly A. Magrini: 0000-0002-0216-7424

Author Contributions

The manuscript was written through contributions from all authors. All authors have given approval to the final version of the manuscript.

Funding

Funding was provided by the U.S. Department of Energy's Office of Energy Efficiency and Renewable Energy (EERE) under Bioenergy Technologies Office (BETO).

Notes

The authors declare no competing financial interest.

ACKNOWLEDGMENTS

This work was authored by Alliance for Sustainable Energy, LLC, the manager and operator of the National Renewable Energy Laboratory for the U.S. Department of Energy (DOE) under Contract No. DE-AC36-08GO28308. Funding was provided by the U.S. Department of Energy's Office of Energy Efficiency and Renewable Energy (EERE) under Bioenergy Technologies Office (BETO). The views expressed in the article do not necessarily represent the views of the DOE or the U.S. Government. The U.S. Government retains and the publisher, by accepting the article for publication, acknowledges that the U.S. Government retains a nonexclusive, paid-up, irrevocable, worldwide license to publish or reproduce the published form of this work, or allow others to do so, for U.S. Government purposes. The authors would like to thank Matthew Coats, Richard French, Jessica Olstad, and Michael Sprague for analytical support and as well as for offering subject-matter expertise.

ABBREVIATIONS

HGF, hot-gas filtration; CHGF, catalytic hot-gas filtration; CFP, catalytic fast pyrolysis; HPA, heteropolyacid; HDO, hydrodeoxygenation; MBMS, molecular beam mass spectrometer; FCT, fractional condensation train; TOS, time-on-stream; ESP, electrostatic precipitator; DCR, Davison circulating riser; LEV, local exhaust ventilation; WHSV, weight-hourly space velocity; BTX, benzene, toluene, and xylene

DOI: 10.1021/acssuschemeng.9b03188
ACS Sustainable Chem. Eng. XXXX, XXX, XXX−XXX

REFERENCES

(1) Ciesielski, P. N.; Pecha, M. B.; Bharadwaj, V. S.; Mukarakate, C.; Leong, G. J.; Kappes, B.; Crowley, M. F.; Kim, S.; Foust, T. D.; Nimlos, M. R. Advancing catalytic fast pyrolysis through integrated multiscale modeling and experimentation: Challenges, progress, and perspectives. *Wires. Energy Environ.* **2018**, *7* (4), 1−19.

(2) Krutof, A.; Hawboldt, K. A. Upgrading of biomass sourced pyrolysis oil review: focus on co-pyrolysis and vapour upgrading during pyrolysis. *Biomass Convers. Biorefin.* **2018**, *8* (3), 775−787.

(3) Luo, G.; Resende, F. L. P. In-situ and ex-situ upgrading of pyrolysis vapors from beetle-killed trees. *Fuel* **2016**, *166*, 367−375.

(4) Mante, O. D.; Dayton, D. C.; Carpenter, J. R.; Wang, K.; Peters, J. E. Pilot-scale catalytic fast pyrolysis of loblolly pine over γ-Al2O3 catalyst. *Fuel* **2018**, *214*, 569−579.

(5) Rahman, M. M.; Liu, R.; Cai, J. Catalytic fast pyrolysis of biomass over zeolites for high quality bio-oil - A review. *Fuel Process. Technol.* **2018**, *180*, 32−46.

(6) Saraeian, A.; Nolte, M. W.; Shanks, B. H. Deoxygenation of biomass pyrolysis vapors: Improving clarity on the fate of carbon. *Renewable Sustainable Energy Rev.* **2019**, *104*, 262−280.

(7) Wang, K.; Dayton, D. C.; Peters, J. E.; Mante, O. D. Reactive catalytic fast pyrolysis of biomass to produce high-quality bio-crude. *Green Chem.* **2017**, *19* (14), 3243−3251.

(8) Ruddy, D. A.; Schaidle, J. A.; Ferrell, J. R., Iii; Wang, J.; Moens, L.; Hensley, J. E. Recent advances in heterogeneous catalysts for bio-oil upgrading via "ex situ catalytic fast pyrolysis": Catalyst development through the study of model compounds. *Green Chem.* **2014**, *16* (2), 454−490.

(9) Mukarakate, C.; Zhang, X.; Stanton, A. R.; Robichaud, D. J.; Ciesielski, P. N.; Malhotra, K.; Donohoe, B. S.; Gjersing, E.; Evans, R. J.; Heroux, D. S.; Richards, R.; Iisa, K.; Nimlos, M. R. Real-time monitoring of the deactivation of HZSM-5 during upgrading of pine pyrolysis vapors. *Green Chem.* **2014**, *16* (3), 1444−1461.

(10) Yung, M. M.; Starace, A. K.; Griffin, M. B.; Wells, J. D.; Patalano, R. E.; Smith, K. R.; Schaidle, J. A. Restoring ZSM-5 performance for catalytic fast pyrolysis of biomass: Effect of regeneration temperature. *Catal. Today* **2019**, *323*, 76−85.

(11) Alsbou, E.; Helleur, B. Accelerated aging of bio-oil from fast pyrolysis of hardwood. *Energy Fuels* **2014**, *28* (5), 3224−3235.

(12) Baldwin, R. M.; Feik, C. J. Bio-oil stabilization and upgrading by hot gas filtration. *Energy Fuels* **2013**, *27* (6), 3224−3238.

(13) Bridgwater, A. V. Upgrading biomass fast pyrolysis liquids. *Environ. Prog. Sustainable Energy* **2012**, *31* (2), 261−268.

(14) Elliott, D. C.; Oasmaa, A.; Preto, F.; Meier, D.; Bridgwater, A. V. Results of the IEA round robin on viscosity and stability of fast pyrolysis bio-oils. *Energy Fuels* **2012**, *26* (6), 3769−3776.

(15) Huber, G. W.; Iborra, S.; Corma, A. Synthesis of transportation fuels from biomass: Chemistry, catalysts, and engineering. *Chem. Rev.* **2006**, *106*, 4044−4098.

(16) Ruiz, M.; Martin, E.; Blin, J.; Van De Steene, L.; Broust, F. Understanding the secondary reactions of flash pyrolysis vapors inside a hot gas filtration unit. *Energy Fuels* **2017**, *31* (12), 13785−13795.

(17) Tomasi Morgano, M.; Leibold, H.; Richter, F.; Seifert, H. Screw pyrolysis with integrated sequential hot gas filtration. *J. Anal. Appl. Pyrolysis* **2015**, *113*, 216−224.

(18) Oasmaa, A.; Elliott, D. C.; Korhonen, J. Acidity of biomass fast pyrolysis bio-oils. *Energy Fuels* **2010**, *24* (12), 6548−6554.

(19) Kumar, R.; Enjamuri, N.; Shah, S.; Al-Fatesh, A. S.; Bravo-Suárez, J. J.; Chowdhury, B. Ketonization of oxygenated hydrocarbons on metal oxide based catalysts. *Catal. Today* **2018**, *302*, 16−49.

(20) Pham, T. N.; Sooknoi, T.; Crossley, S. P.; Resasco, D. E. Ketonization of carboxylic acids: Mechanisms, catalysts, and implications for biomass conversion. *ACS Catal.* **2013**, *3* (11), 2456−2473.

(21) Pacchioni, G. Ketonization of carboxylic acids in biomass conversion over TiO2 and ZrO2 surfaces: A DFT perspective. *ACS Catal.* **2014**, *4* (9), 2874−2888.

(22) Bayahia, H. Gas-phase ketonization of acetic acid over Co-Mo and its supported catalysts. *J. Taibah Univ. Sci.* **2018**, *12* (2), 191−196.

(23) Lu, F.; Jiang, B.; Wang, J.; Huang, Z.; Liao, Z.; Yang, Y.; Zheng, J. Promotional effect of Ti doping on the ketonization of acetic acid over a CeO2 catalyst. *RSC Adv.* **2017**, *7* (36), 22017−22026.

(24) Chan, W. P.; Veksha, A.; Lei, J.; Oh, W. D.; Dou, X.; Giannis, A.; Lisak, G.; Lim, T. T. A hot syngas purification system integrated with downdraft gasification of municipal solid waste. *Appl. Energy* **2019**, *237*, 227−240.

(25) Dutta, A.; Schaidle, J. A.; Humbird, D.; Baddour, F. G.; Sahir, A. Conceptual process design and techno-economic assessment of ex situ catalytic fast pyrolysis of biomass: A fixed bed reactor implementation scenario for future feasibility. *Top. Catal.* **2016**, *59* (1), 2−18.

(26) Heidenreich, S. Hot gas filtration - A review. *Fuel* **2013**, *104*, 83−94.

(27) Heidenreich, S.; Foscolo, P. U. New concepts in biomass gasification. *Prog. Energy Combust. Sci.* **2015**, *46*, 72−95.

(28) Nacken, M.; Ma, L.; Engelen, K.; Heidenreich, S.; Baron, G. V. Development of a tar reforming catalyst for integration in a ceramic filter element and use in hot gas cleaning. *Ind. Eng. Chem. Res.* **2007**, *46* (7), 1945−1951.

(29) Nacken, M.; Ma, L.; Heidenreich, S.; Baron, G. V. Performance of a catalytically activated ceramic hot gas filter for catalytic tar removal from biomass gasification gas. *Appl. Catal., B* **2009**, *88* (3), 292−298.

(30) Nacken, M.; Ma, L.; Heidenreich, S.; Verpoort, F.; Baron, G. V. Development of a catalytic ceramic foam for efficient tar reforming of a catalytic filter for hot gas cleaning of biomass-derived syngas. *Appl. Catal., B* **2012**, *125*, 111−119.

(31) Rapagnà, S.; Gallucci, K.; Di Marcello, M.; Matt, M.; Nacken, M.; Heidenreich, S.; Foscolo, P. U. Gas cleaning, gas conditioning and tar abatement by means of a catalytic filter candle in a biomass fluidized-bed gasifier. *Bioresour. Technol.* **2010**, *101* (18), 7123−7130.

(32) Shen, Y.; Yoshikawa, K. Recent progresses in catalytic tar elimination during biomass gasification or pyrolysis—A review. *Renewable Sustainable Energy Rev.* **2013**, *21*, 371−392.

(33) Turan, A. Z.; Cetin, Y.; Tuna, Ö.; Sarıoglan, A. Development of calcium silicate-based catalytic filters for biomass fuel gas reforming. *Int. J. Energy Res.* **2019**, *43* (3), 1217−1231.

(34) Johansson, A.-C.; Iisa, K.; Sandström, L.; Ben, H.; Pilath, H.; Deutch, S.; Wiinikka, H.; Öhrman, O. G. W. Fractional condensation of pyrolysis vapors produced from Nordic feedstocks in cyclone pyrolysis. *J. Anal. Appl. Pyrolysis* **2017**, *123*, 244−254.

(35) Kim, P.; Weaver, S.; Noh, K.; Labbé, N. Characteristics of bio-oils produced by an intermediate semipilot scale pyrolysis auger reactor equipped with multistage condensers. *Energy Fuels* **2014**, *28* (11), 6966−6973.

(36) Ma, S.; Zhang, L.; Zhu, L.; Zhu, X. Preparation of multipurpose bio-oil from rice husk by pyrolysis and fractional condensation. *J. Anal. Appl. Pyrolysis* **2018**, *131*, 113−119.

(37) Schulzke, T.; Conrad, S.; Westermeyer, J. Fractionation of flash pyrolysis condensates by staged condensation. *Biomass Bioenergy* **2016**, *95*, 287−295.

(38) Sui, H.; Yang, H.; Shao, J.; Wang, X.; Li, Y.; Chen, H. Fractional condensation of multicomponent vapors from pyrolysis of cotton stalk. *Energy Fuels* **2014**, *28* (8), 5095−5102.

(39) Westerhof, R. J. M.; Brilman, D. W. F.; Garcia-Perez, M.; Wang, Z.; Oudenhoven, S. R. G.; Van Swaaij, W. P. M.; Kersten, S. R. A. Fractional condensation of biomass pyrolysis vapors. *Energy Fuels* **2011**, *25* (4), 1817−1829.

(40) Westerhof, R. J. M.; Kuipers, N. J. M.; Kersten, S. R. A.; Swaaij, W. P. M. v. Controlling the water content of biomass fast pyrolysis oil. *Ind. Eng. Chem. Res.* **2007**, *46*, 9238−9247.

(41) Pollard, A. S.; Rover, M. R.; Brown, R. C. Characterization of bio-oil recovered as stage fractions with unique chemical and physical properties. *J. Anal. Appl. Pyrolysis* **2012**, *93*, 129−138.

DOI: 10.1021/acssuschemeng.9b03188
ACS Sustainable Chem. Eng. XXXX, XXX, XXX−XXX

(42) Grossman, A.; Vermerris, W. Lignin-based polymers and nanomaterials. *Curr. Opin. Biotechnol.* **2019**, *56*, 112−120.
(43) Parsell, T.; Yohe, S.; Degenstein, J.; Jarrell, T.; Klein, I.; Gencer, E.; Hewetson, B.; Hurt, M.; Kim, J. I.; Choudhari, H.; Saha, B.; Meilan, R.; Mosier, N.; Ribeiro, F.; Delgass, W. N.; Chapple, C.; Kenttämaa, H. I.; Agrawal, R.; Abu-Omar, M. M. A synergistic biorefinery based on catalytic conversion of lignin prior to cellulose starting from lignocellulosic biomass. *Green Chem.* **2015**, *17* (3), 1492−1499.
(44) Wang, S.-S.; Yang, G.-Y. Recent advances in polyoxometalate-catalyzed reactions. *Chem. Rev.* **2015**, *115* (11), 4893−4962.
(45) Anderson, E.; Crisci, A.; Murugappan, K.; Roman-Leshkov, Y. Bifunctional molybdenum polyoxometalates for the combined hydrodeoxygenation and alkylation of lignin-derived model phenolics. *ChemSusChem* **2017**, *10*, 2226−2234.
(46) Murugappan, K.; Mukarakate, C.; Budhi, S.; Shetty, M.; Nimlos, M. R.; Román-Leshkov, Y. Supported molybdenum oxides as effective catalysts for the catalytic fast pyrolysis of lignocellulosic biomass. *Green Chem.* **2016**, *18* (20), 5548−5557.
(47) Zhang, X.; Chen, Q.; Zhang, Q.; Wang, C.; Ma, L.; Xu, Y. Conversion of pyrolytic lignin to aromatic hydrocarbons by hydrocracking over pristine MoO3 catalyst. *J. Anal. Appl. Pyrolysis* **2018**, *135*, 60−66.
(48) Ranga, C.; Lødeng, R.; Alexiadis, V. I.; Rajkhowa, T.; Bjørkan, H.; Chytil, S.; Svenum, I. H.; Walmsley, J.; Detavernier, C.; Poelman, H.; Van Der Voort, P.; Thybaut, J. W. Effect of composition and preparation of supported MoO3 catalysts for anisole hydrodeoxygenation. *Chem. Eng. J.* **2018**, *335*, 120−132.
(49) Saidi, M.; Samimi, F.; Karimipourfard, D.; Nimmanwudipong, T.; Gates, B. C.; Rahimpour, M. R. Upgrading of lignin-derived bio-oils by catalytic hydrodeoxygenation. *Energy Environ. Sci.* **2014**, *7* (1), 103−129.
(50) Shetty, M.; Murugappan, K.; Green, W. H.; Román-Leshkov, Y. Structural properties and reactivity trends of molybdenum oxide catalysts supported on zirconia for the hydrodeoxygenation of anisole. *ACS Sustainable Chem. Eng.* **2017**, *5* (6), 5293−5301.
(51) Hornebecq, V.; Mastai, Y.; Antonietti, M.; Polarz, S. Redox behavior of nanostructured molybdenum oxide-mesoporous silica hybrid materials. *Chem. Mater.* **2003**, *15* (19), 3586−3593.
(52) Li, X.; Pang, J.; Zhang, J.; Yin, C.; Zou, W.; Tang, C.; Dong, L. Vapor-phase deoxygenation of lactic acid to biopropionic acid over dispersant-enhanced molybdenum oxide catalyst. *Ind. Eng. Chem. Res.* **2019**, *58* (1), 101−109.
(53) Ranga, C.; Alexiadis, V. I.; Lauwaert, J.; Lødeng, R.; Thybaut, J. W. Effect of Co incorporation and support selection on deoxygenation selectivity and stability of (Co)Mo catalysts in anisole HDO. *Appl. Catal., A* **2019**, *571*, 61−70.
(54) Zhao, A.; Masa, J.; Xia, W. Oxygen-deficient titania as alternative support for Pt catalysts for the oxygen reduction reaction. *J. Energy Chem.* **2014**, *23*, 701−707.
(55) Mukarakate, C.; Watson, M. J.; ten Dam, J.; Baucherel, X.; Budhi, S.; Yung, M. M.; Ben, H.; Iisa, K.; Baldwin, R. M.; Nimlos, M. R. Upgrading biomass pyrolysis vapors over β-zeolites: role of silica-to-alumina ratio. *Green Chem.* **2014**, *16* (12), 4891−4905.
(56) Atia, H.; Armbruster, U.; Martin, A. Dehydration of glycerol in gas phase using heteropolyacid catalysts as active compounds. *J. Catal.* **2008**, *258* (1), 71−82.
(57) Byrne, C.; Moran, L.; Hermosilla, D.; Merayo, N.; Blanco, Á.; Rhatigan, S.; Hinder, S.; Ganguly, P.; Nolan, M.; Pillai, S. C. Effect of Cu doping on the anatase-to-rutile phase transition in TiO_2 photocatalysts: Theory and experiments. *Appl. Catal., B* **2019**, *246*, 266−276.
(58) Nair, V.; Vinu, R. Production of guaiacols via catalytic fast pyrolysis of alkali lignin using titania, zirconia and ceria. *J. Anal. Appl. Pyrolysis* **2016**, *119*, 31−39.
(59) Black, B. A.; Michener, W. E.; Ramirez, K. J.; Biddy, M. J.; Knott, B. C.; Jarvis, M. W.; Olstad, J.; Mante, O. D.; Dayton, D. C.; Beckham, G. T. Aqueous stream characterization from biomass fast pyrolysis and catalytic fast pyrolysis. *ACS Sustainable Chem. Eng.* **2016**, *4* (12), 6815−6827.
(60) Guda, V. K.; Toghiani, H. Catalytic pyrolysis of pinewood using metal oxide catalysts in an integrated reactor system. *Biofuels* **2017**, *8* (5), 527−536.
(61) Mante, O. D.; Rodriguez, J. A.; Babu, S. P. Selective defunctionalization by TiO2 of monomeric phenolics from lignin pyrolysis into simple phenols. *Bioresour. Technol.* **2013**, *148*, 508−516.
(62) Silbaugh, T. L.; Boaventura, J. S.; Barteau, M. A. Surface acidity scales: Experimental measurements of Brønsted acidities on anatase TiO2 and comparison with coinage metal surfaces. *Surf. Sci.* **2016**, *650*, 64−70.
(63) Wang, S.; Goulas, K.; Iglesia, E. Condensation and esterification reactions of alkanals, alkanones, and alkanols on TiO2: Elementary steps, site requirements, and synergistic effects of bifunctional strategies. *J. Catal.* **2016**, *340*, 302−320.
(64) Wang, S.; Iglesia, E. Experimental and theoretical assessment of the mechanism and site requirements for ketonization of carboxylic acids on oxides. *J. Catal.* **2017**, *345*, 183−206.
(65) Mukarakate, C.; McBrayer, J. D.; Evans, T. J.; Budhi, S.; Robichaud, D. J.; Iisa, K.; ten Dam, J.; Watson, M. J.; Baldwin, R. M.; Nimlos, M. R. Catalytic fast pyrolysis of biomass: The reactions of water and aromatic intermediates produces phenols. *Green Chem.* **2015**, *17* (8), 4217−4227.
(66) Jendoubi, N.; Broust, F.; Commandre, J. M.; Mauviel, G.; Sardin, M.; Lédé, J. Inorganics distribution in bio oils and char produced by biomass fast pyrolysis: The key role of aerosols. *J. Anal. Appl. Pyrolysis* **2011**, *92*, 59−67.
(67) Kang, B.-S.; Lee, K. H.; Park, H. J.; Park, Y.-K.; Kim, J.-S. Fast pyrolysis of radiata pine in a bench scale plant with a fluidized bed: Influence of a char separation system and reaction conditions on the production of bio-oil. *J. Anal. Appl. Pyrolysis* **2006**, *76* (1), 32−37.
(68) Karnowo; Zahara, Z. F.; Kudo, S.; Norinaga, K.; Hayashi, J.-i. Leaching of alkali and alkaline earth metallic species from rice husk with bio-oil from its pyrolysis. *Energy Fuels* **2014**, *28* (10), 6459−6466.
(69) Mei, Y.; Liu, R. Effect of temperature of ceramic hot vapor filter in a fluidized bed reactor on chemical composition and structure of bio-oil and reaction mechanism of pine sawdust fast pyrolysis. *Fuel Process. Technol.* **2017**, *161*, 204−219.
(70) Zhang, M.; Wu, H. Bioslurry as a fuel. 6. Leaching characteristics of alkali and alkaline Earth metallic species from biochar by bio-oil model compounds. *Energy Fuels* **2015**, *29* (4), 2535−2541.
(71) Papari, S.; Hawboldt, K. A review on condensing system for biomass pyrolysis process. *Fuel Process. Technol.* **2018**, *180*, 1−13.
(72) Moens, L.; Black, S. K.; Myers, M. D.; Czernik, S. Study of the neutralization and stabilization of a mixed hardwood bio-oil. *Energy Fuels* **2009**, *23*, 2695−2699.
(73) Diebold, J. *A review of the chemical and physical mechanisms of the storage stability of fast pyrolysis bio-oils*. National Renewable Energy Laboratory (NREL): Golden, CO, 1999; DOI: 10.2172/753818.
(74) Snell, R. W.; Combs, E.; Shanks, B. H. Aldol condensations using bio-oil model compounds: The role of acid-base bi-functionality. *Top. Catal.* **2010**, *53* (15−18), 1248−1253.
(75) Black, S.; Ferrell, J. R. Determination of carbonyl groups in pyrolysis bio-oils using potentiometric titration: Review and comparison of methods. *Energy Fuels* **2016**, *30*, 1071−1077.
(76) Rover, M. R.; Johnston, P. A.; Whitmer, L. E.; Smith, R. G.; Brown, R. C. The effect of pyrolysis temperature on recovery of bio-oil as distinctive stage fractions. *J. Anal. Appl. Pyrolysis* **2014**, *105*, 262−268.
(77) Meng, J.; Moore, A.; Tilotta, D.; Kelley, S.; Park, S. Toward understanding of bio-oil aging: Accelerated aging of bio-oil fractions. *ACS Sustainable Chem. Eng.* **2014**, *2* (8), 2011−2018.
(78) Iisa, K.; French, R. J.; Orton, K. A.; Dutta, A.; Schaidle, J. A. Production of low-oxygen bio-oil via ex situ catalytic fast pyrolysis and hydrotreating. *Fuel* **2017**, *207*, 413−422.

DOI: 10.1021/acssuschemeng.9b03188
ACS Sustainable Chem. Eng. XXXX, XXX, XXX−XXX